16th Australasian Fluid Mechanics Conference
Crown Plaza, Gold Coast, Australia
2-7 December 2007

Some Insights into Synthetic Jet Actuation From Analytical Modelling

R.N. Sharma

Department of Mechanical Engineering
The University of Auckland, Auckland 1142, NEW ZEALAND

Abstract

An analytical model based on the laws of fluid dynamics for synthetic jet actuation into quiescent air as well as into external flow fields is presented. A synthetic jet actuator consists of a cavity with a driven wall and an orifice. Under actuation, the wall is oscillated resulting in an oscillatory flow through the orifice. In the model, the driven wall is modelled as a single degree of freedom mechanical system, which is pneumatically coupled to the cavity-orifice arrangement acting as a Helmholtz resonator. The latter has been modelled using the unsteady form of the continuity and Bernoulli equations with a loss term. External flow field effects are represented by fluctuating external pressure at the actuator orifice. The model has been validated against experimental data available in the published literature, and excellent agreement is obtained between the predicted and measured frequency responses as well as the phase relationships between velocities and pressures. The model and analysis based on it provides valuable insights into the behaviour of synthetic jet actuators, and reveals amongst other things, that air in the actuator cavity exhibits compressibility at all frequencies beyond the Helmholtz resonance frequency. Furthermore, the actuator output velocity is maximised when cavity Helmholtz and wall natural frequencies are brought together. The presence of an external flow field could either aid or hinder actuation depending on the phase relationship between, and the relative frequencies of, the wall forcing and external pressure fluctuations.

Introduction

A 'synthetic jet' is a quasi-steady jet of air generated a few diameters from the orifice of a 'synthetic jet actuator', as illustrated in Figure 1. Actuation involves the forcing of an oscillatory air-flow through the orifice from a cavity with a driven flexible wall [1]. During out-flow, an air jet is formed directly in front of the orifice, accompanied by a vortex ring around the orifice which is shed as out-flow weakens and reverts to in-flow. Since the in-flow part of the oscillatory cycle entrains air from around the shed vortex ring, the flow-field established some distance downstream of the orifice is relatively undisturbed and the shed vortices are not destructed, leading to the maintenance of a quasi-steady or synthetic jet. The train of vortex rings that are periodically shed and advected away from the orifice, eventually break down in the region of this synthetic jet, thus intermittently transporting momentum to and thereby sustaining the jet [2].

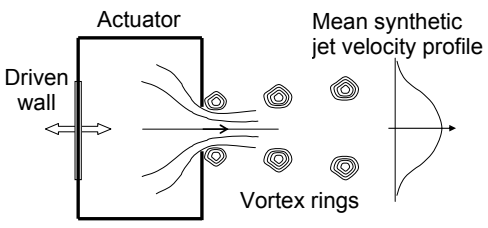

Figure 1. Synthetic jet actuation

A major advantage of the synthetic jet over the ordinary steady jet is that it does not require a continuous supply of air from elsewhere for the maintenance of the jet, since the jet is synthesised from the surrounding fluid. Consequently, the actuator has advantages of simple structure, low cost and easy installation. The synthetic jet has thus attracted much research within the last decade and a comprehensive review will be found in Glezer and Amitay [3]. Past investigations into applications of synthetic jets range from thrust vectoring of jet engines [4], through mixing enhancement [5], to external flow boundary layer separation control [6]. A number of studies (for example Smith [7]), have focussed upon the interaction of synthetic jets with boundary layer cross-flows. Benchiekh et al. [8] and Amitay et al. [9] have attempted the control of separation in internal flows, in particular inside a diffuser, with some measure of success. Synthetic jets can also enhance heat and mass transfer [10, 11].

While understanding of the evolution and characteristics of synthetic jets are important in the development of its applications, the actuation and optimisation of actuators are equally as important. Mallinson et al. [12] have shown that the resultant jet shows evidence of the influence of acoustic resonance of the cavity and structural resonance of the flexible wall. Guy et al. [13, 14] show that the output of the actuator is maximised at the two resonance frequencies. Furthermore, it is suggested that there is an optimum combination of all geometric parameters at which the actuator will operate at its full capacity. Gallas et al. [15-17] offered a lumped element model (LEM) based upon an analogy with electrical circuitry, in which the components of a piezo-electrically driven synthetic jet actuator are modelled as elements of an equivalent electrical circuit. The writers discussed methods of estimation of model parameters and provided experimental verification of their model. Agreement between the model and experimental data was found to be good, allowing some measure of optimisation of the actuator. Gallas et al. [18] also found that the actuator orifice flow is characterised by linear and non-linear losses depending upon oscillating wall stroke lengths relative to the orifice size; however they conclude that further investigation is required to develop correlations for orifice loss coefficients as functions of Reynolds number and wall stroke lengths. Recently, Sharma [19-20] has offered an alternative synthetic jet actuation model based on the laws of fluid dynamics, validated against experimental data available in the published literature.

The purpose of this paper is to amalgamate the analytical models of Sharma [19-20] and then to use it to gain further insight into the behaviour of synthetic jet actuators; and to improve the understanding of the performance of the actuator and its sensitivity to changes of important design parameters.

Analytical Model

The analytical model of Sharma [19-20] considers the actuation of the cavity wall of a typical synthetic jet actuator through an input supply voltage, as illustrated in the schematic of Figure 2.

The actuator is assumed to interact with either quiescent air or with an external flow-field represented by an orifice external fluctuating pressure $p_e(t)$. The model relates the output of the actuator, namely the orifice flow velocity $U(t)$, and also the actuator cavity internal pressure $p_i(t)$, to the driving force $F(t)$

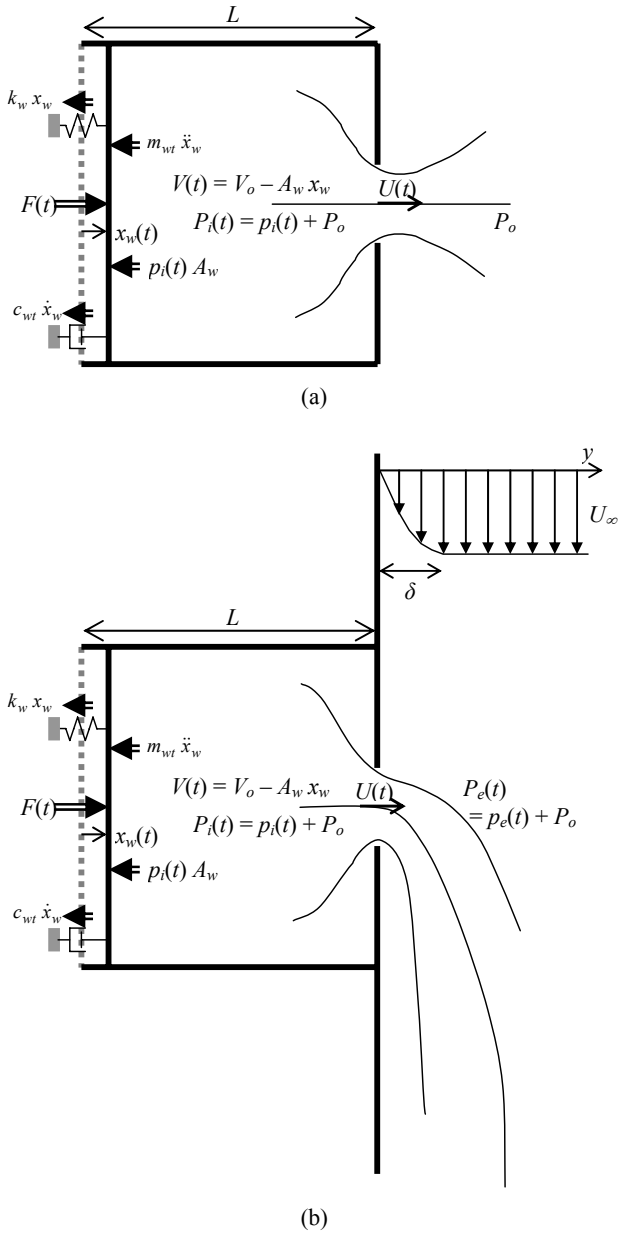

Figure 2. Synthetic jet actuation (a) into quiescent air, and (b) into a cross flow boundary layer; NB: Dotted line represents original wall position; and P_O = atmospheric pressure

effected through an input voltage $v(t)$, and to the external pressure signal $p_e(t)$. We assume that $F(t)$ is some known function of $v(t)$ and the characteristics of the actuation mechanism Z,

$$F(t) = g\left(v(t), Z\right) \tag{1}$$

The oscillating wall of the actuator could take one of a number of different forms, such as a piezo-electrically driven diaphragm, a mechanically driven piston or mechanically driven diaphragm. For example, $F(t)$ could be an electro-dynamic force generated with varying input voltage $v(t)$ such as that in an audio speaker mechanism.

In the model, the flexible wall is consider to behave as a piston where it is deemed to displace as a rigid body in one dimension. An audio speaker displays such a behaviour in the middle to low frequency range (Kinsler et al. [21]; page 410) since the speed of transverse waves is about 500m/s. Consequently, it is reasonable to assume that the speaker cone moves as a unit for frequencies below 500Hz. From a mechanical systems point of view, a piezo-electrically driven diaphragm displays behaviour similar to that of a single degree of freedom system [15-17]. In this way, the driven wall of a synthetic jet actuator is readily modelled as a mechanical mass-damper-stiffness system having a mass m_w, damping coefficient c_w, and stiffness k_w. An added mass term m_a representing added air mass would be significant if the diaphragm or driven wall is lightweight. In addition, an acoustic radiation damping force $c_a\dot{x}_w$ could be expected. Under actuation, the gauge pressure inside the cavity $p_i(t)$ will fluctuate about a zero mean value as the air undergoes compression and expansion. Consequently, an equation governing the dynamics of the flexible membrane may thus be obtained under the action of the electromotive and internal pressure forces as

$$m_{wt}\,\ddot{x}_w \;+\; c_{wt}\,\dot{x}_w \;+\; k_w\,x_w \;=\; F \;-\; p_i\,A_w \tag{2a}$$

in which $A_w = \pi d_w^2/4$ is the area of the flexible wall, $x_w(t)$ is its displacement, and m_{wt} and c_{wt} are the total mass $m_{wt} = m_w + m_a$ and damping coefficient $c_{wt} = c_w + c_a$.

For a circular piston vibrating in an infinite baffle at cyclic frequency f or radian frequency $\omega = 2\pi f$, the added mass and damping terms are [21]

$$m_a \;=\; \rho_a A_w U_S X_1(y)/\omega \quad \text{and} \quad c_a \;=\; \rho_a A_w U_S R_1(y) \tag{2b}$$

where the functions $X_1(y)$ and $R_1(y)$ are defined in terms of the Struve function of the first kind $H_1(y)$ and the first order Bessel function of the first kind $J_1(y)$ respectively, as follows

$$y \;=\; \omega d_w / U_S \tag{2c}$$

$$X_1(y) = 2\,\mathrm{H}_1(y)/\,y = (4/\pi)\left(y/3 - y^3/(3^2\cdot 5) + y^5/(3^2\cdot 5^2\cdot 7) - \cdots\right) \tag{2d}$$

$$R_1(y) = 1 - 2J_1(y)/\,y = y^2/(2\cdot 4) - y^4/(2\cdot 4^2\cdot 6) + y^6/(2\cdot 4^2\cdot 6^2\cdot 8) - \cdots \tag{2e}$$

for $y < 1$. For a small actuator having a 10mm diameter diaphragm operating in ambient conditions, the $y < 1$ restriction on Equations (2d) and (2e) means that these will give converged results for frequencies below approximately 5.5kHz. Synthetic jet actuators are typically operated below this frequency, see for example Gallas et al. [15-17].

Equation (2a) may be re-written as

$$\ddot{x}_w + 2\varsigma_w\,\omega_w\,\dot{x}_w + \omega_w^2\,x_w = F/m_{wt} - p_i A_w/m_{wt} \tag{3}$$

in which

$$\varsigma_w \;=\; c_{wt}/2\sqrt{m_{wt}\,k_w} \tag{4}$$

and

$$\omega_w \;=\; \sqrt{k_w/m_{wt}} \;=\; 2\pi f_w \tag{5}$$

These parameters will depend upon the structural characteristics of the wall, and the manner in which it is supported.

When the wall is oscillated, air inside the cavity undergoes alternate compression and expansion with an accompanying oscillatory flow through the orifice. The continuity equation for the actuator can thus be written as [19]

$$V_o\,(dp_i/dt)/(\gamma P_o) - A_w\,\dot{x}_w = -A_o\,U \tag{6}$$

Considering the orifice outflow and inflow parts of the actuation cycle as illustrated in Figure 3, application of the unsteady form of the Bernoulli equation [19-20] leads to

$$p_i = p_e + K\,\tfrac{1}{2}\rho_a\,|U|U + \rho_a\,l_e\,(dU/dt) \tag{7}$$

In Equation (7), K is an effective loss-coefficient defining the losses through the orifice, and l_e is an effective length that defines the inertia of the air jet moving through the orifice. Under steady conditions, the loss coefficient may be taken as 0.42 corresponding to a sudden contraction [19-20].

Values for the effective length may be estimated using data available in the acoustics literature, (e.g. see Hall [22]), or from studies on building internal pressure dynamics induced through openings [23-26]. The effective length of the air jet / slug at the orifice is a sum of the actual orifice length l_o and end corrections quantified using an inertia coefficient C_I, such that

$$l_e = l_o + C_I\sqrt{A_o} \tag{8}$$

Equations (7) and (8) may now be combined. Eliminating the orifice flow velocity U leads to an equation governing the dynamics of internal pressure,

$$\begin{aligned}&\ddot{p}_i + V_o K/(2\gamma A_o P_o l_e)\,|\dot{p}_i - (\gamma A_w P_o/V_o)\,\dot{x}_w| \\ &\times(\dot{p}_i - (\gamma A_w P_o/V_o)\,\dot{x}_w) + \omega_h^2\,p_i = (\gamma A_w P_o/V_o)\,\ddot{x}_w + \omega_h^2\,p_e\end{aligned} \tag{9a}$$

$$\begin{aligned}&\ddot{p}_i + V_o K/(2\gamma A_o P_o l_e)\,|\dot{p}_i - (m_w\omega_{wp}^2/A_w)\,\dot{x}_w| \\ &\times(\dot{p}_i - (m_w\omega_{wp}^2/A_w)\,\dot{x}_w) + \omega_h^2\,p_i = (m_w\omega_{wp}^2/A_w)\,\ddot{x}_w + \omega_h^2\,p_e\end{aligned} \tag{9b}$$

However, if we chose to eliminate internal pressure p_i then an equation governing the dynamics of the mean orifice flow velocity is obtained,

$$\begin{aligned}&\ddot{U} + (K/l_e)\,|U|\dot{U} + \omega_h^2\,U \\ &\quad = (\gamma\,A_w\,P_o/(\rho_a\,l_e\,V_o))\,\dot{x}_w - \dot{p}_e/(\rho\,l_e)\end{aligned} \tag{10a}$$

$$\ddot{U} + (K/l_e)\,|U|\dot{U} + \omega_h^2\,U = (A_w/A_o)\,\omega_h^2\,\dot{x}_w - \dot{p}_e/(\rho\,l_e) \tag{10b}$$

In Equations (9-10),

$$\begin{aligned}\omega_h = 2\pi f_h &= \sqrt{k_h/m_h} = \sqrt{(\gamma A_o^2 P_o/V_o)/(\rho_a l_e A_o)} \\ &= \sqrt{(\gamma A_o P_o)/(\rho_a l_e V_o)} = U_S\sqrt{A_o/(l_e V_o)}\end{aligned} \tag{11}$$

is the Helmholtz resonance frequency of the cavity with the orifice; and

$$\omega_{wp} = \sqrt{k_{wp}/m_w} = \sqrt{(\gamma A_w^2 P_o/V_o)/m_w} \tag{12}$$

is the natural frequency of the pneumatic spring made of the oscillatory wall of mass m_w against a sealed cavity volume V_o. Equations (9) and (10) are those for a Helmholtz acoustic resonator, as noted and discussed previously [18-20], with pneumatic coupling to the dynamics of the oscillating wall. The synthetic jet actuator is therefore viewed as a coupled mechanical (dynamic wall) – Helmholtz resonator system with two degrees of freedom, as discussed previously. If we make the wall rigid and therefore set the time derivatives of x_w to zero, then the Helmholtz resonator equation is retrieved with an external pressure excitation term,

$$\ddot{p}_i + V_o K/(2\gamma A_o P_o l_e)\,|\dot{p}_i|\,\dot{p}_i + \omega_h^2\,p_i = \omega_h^2\,p_e \tag{13a}$$

$$\ddot{U} + (K/l_e)\,|U|\dot{U} + \omega_h^2\,U = \dot{p}_e/(\rho\,l_e) \tag{13b}$$

The coupled Equations (3, 6, 7, 9 and 10) constitute the synthetic jet actuator model, which relates the input forcing voltage $v(t)$ and the external flow excitation pressure function $p_e(t)$ to the oscillating wall displacement $x_w(t)$, cavity internal pressure $p_i(t)$, and the actuator output or orifice velocity $U(t)$. Since Equations (7, 9-10) are non-linear, a numerical solution scheme has to be employed in order to solve for these variables, for given forcing functions $v(t)$ and $p_e(t)$. In this study, a 4th order Runge-Kutta scheme [27] was employed. In order to implement this numerical solution procedure, the set of equations are re-written as follows

$$p_i = \dot{p}_i\,dt\,,\quad x_w = \dot{x}_w\,dt\,,\quad \dot{x}_w = \ddot{x}_w\,dt\,,\quad U = \dot{U}\,dt \tag{14a}$$

$$\dot{p}_i = (\gamma\,A_w\,P_o/V_o)\,\dot{x}_w - (\gamma\,A_o\,P_o/V_o)\,U \tag{14b}$$

$$\dot{U} = p_i/(\rho\,l_e) - p_e/(\rho\,l_e) - (K/2l_e)\,|U|U \tag{14c}$$

$$\ddot{x}_w = F/m_{wt} - p_i\,A_w/m_{wt} - 2\varsigma_w\,\omega_w\,\dot{x}_w - \omega_w^2\,x_w \tag{14d}$$

An appropriate choice of time-step Δt is made based on the frequency of the forcing and external pressure functions and the solution is then advanced with zero initial conditions.

Model Validation

For validation of the model, the two piezoelectric-driven synthetic jet actuators (I and II) studied by Gallas et al. [15-17] are considered, for which physical and experimental data are available as summarized here in Table 1. Since input to the present model is a sinusoidal force on the diaphragm, the amplitude of this force is estimated using data from references [15-17] in Table 2. Using the effective acoustic piezoelectric coefficient D_a, a volume displacement magnitude ΔV is first calculated for the given forcing voltage amplitude. By equating this to an equivalent volume displacement $\Delta V = A_w x_w$ in the present model, a displacement amplitude results which combined with the wall stiffness yields the force amplitudes of 0.574N and 0.401N for cases I and II respectively. In both cases, actuation is into quiescent air, hence $p_e = 0$.

Component	Property	Case I	Case II
Brass Shim	Density (kg/m^3)	8700	8700
	Thickness (mm)	0.20	0.10
	Diameter (mm)	23.5	37.0
Piezoceramic	Density (kg/m^3)	7700	7700
	Thickness (mm)	0.11	0.10
	Diameter (mm)	20.5	25.0
Diaphragm	Compliance (s^2.m^4/kg)	6.53×10^{-13}	2.23×10^{-11}
	Acoustic mass (kg/m^4)	8.15×10^{3}	2.43×10^{3}
	Acoustic piezoelec. Coeff. d_a (m^3/V)	5.53×10^{-11}	4.32×10^{-10}
	Mechanical damping ratio	0.03	0.03
	Natural frequency (Hz)	2114	632
Cavity	Volume (m^3)	2.5×10^{-6}	5.0×10^{-6}
	Equivalent cylindrical diameter (mm)	23.5	37.0
	Equivalent cylindrical length (mm)	5.76	4.65
Orifice	Diameter (mm)	1.65	0.84
	Length (mm)	1.65	0.84
	Effective loss coefficient	0.78	0.78
	Inertia coefficient	0.705	0.86
	Helmholtz frequency (Hz)	977	473
Forcing	Voltage amplitude (V)	25	25
	Force amplitude (N)	0.574	0.401

Table 1. Properties of piezoelectric-driven synthetic jet actuators of Gallas et al. [15-17]

Figures 3 to 5 compare the maximum orifice velocity predicted by the model with those from the experiment and LEM model of Gallas et al. [15-17], for cases I and II respectively. Figure 3 shows that there is good agreement between the present model and experiment, except in the mid-frequency region where the model over predicts the maximum velocities somewhat. This is similar to the prediction of the LEM model [15-17]. The LEM model on the other hand under predicts the first resonant peak, which clearly relates to the choice of a higher loss coefficient of 1.0 as compared with a value of 0.78 in the present study. The value $K = 0.78$ was chosen as it gave a good match to the peak response. The resonance frequencies of 953Hz and 2184Hz predicted by the model agree quite well with experimental data.

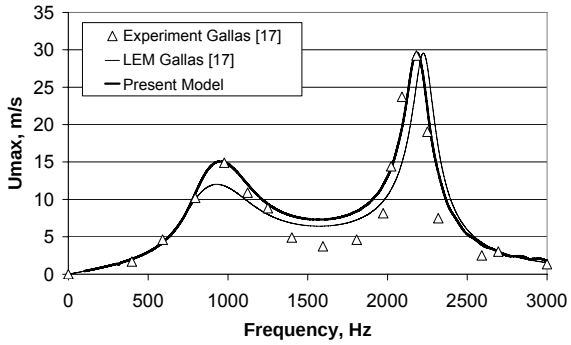

Figure 3. Comparisons between the model, experiment and the LEM [17] for Case I

The sensitivity to the orifice loss coefficient was investigated by computing responses for a range of K values. The results are illustrated in Figure 4, and it shows that the peak responses at both resonances are indeed sensitive to the choice of the orifice loss coefficient K. The orifice loss coefficient K directly determines the losses and thus represents damping in the system. Consequently the peak response of the actuator about the resonance frequencies is sensitive to K. The analysis presented here suggests that K will be somewhat higher than the steady sudden contraction loss coefficient of 0.42, but significantly lower than that for a sharp edged orifice in steady flow. The data here suggests a reasonable range for K values would be between 0.42 and 1.0. Further studies are however warranted to be able to accurately predict this important parameter.

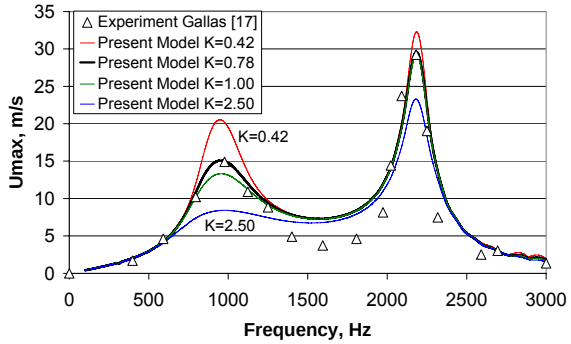

Figure 4. Sensitivity of the actuator output to the orifice loss coefficient K for Case I

In Figure 5 for case II, agreement between the model and experiment is good again. In this case, while the model over predicts the maximum velocities somewhat near the highly damped first resonance, it nevertheless gives a good prediction of the maximum velocity at the resonant peak at 854Hz, with $K = 0.78$. The LEM model with a loss coefficient of 1.0 over predicts the maximum velocity in this case. That this is the case is not surprising as the loss and other orifice coefficients utilised in the present and past studies are taken as constant values, whereas the oscillatory nature of the orifice flow would mean that these are in fact not constant. Clearly, further studies are required to obtain accurate representations for these coefficients. Notwithstanding this, the agreement between the present model and experiment is nevertheless good, which allows the model to be used to investigate actuator performance to important parameters.

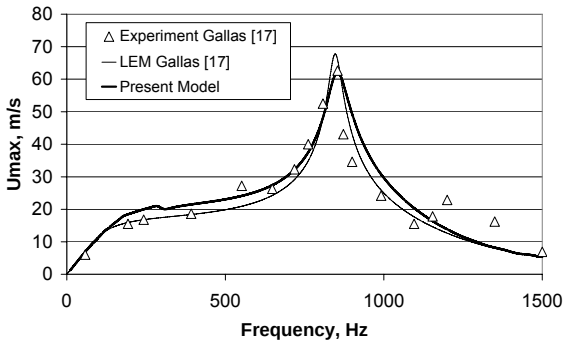

Figure 5. Comparisons between the model, experiment and the LEM [17] for Case II

Diaphragm and Internal Pressure Dynamics

Figure 6 displays the maximum diaphragm displacement and velocity, internal pressure and the orifice velocity calculated using the model for case I. It shows that large amplitude oscillations in internal pressure are obtained within a synthetic jet actuator, which are most enhanced at the resonant frequencies.

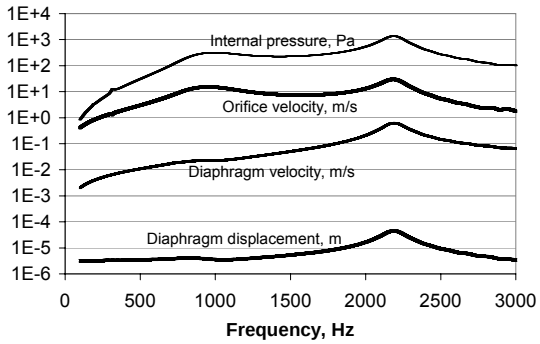

Figure 6. Calculated maximum diaphragm displacement and velocity, internal pressure and orifice velocity for Case I (on a logarithmic scale).

Phase Relationships & Compressibility

Further validation of the new model is provided from a comparison of the calculated phase angles in Figure 7, with experimentally measured data of Gallas et al. [18]. At the very low frequencies, the model shows that the phase angle between the diaphragm velocity and the orifice flow velocity, $\phi_{Vw\text{-}U}$, is near 0° i.e. the two velocities are very nearly in phase, indicating the flow is incompressible. Near the first resonant peak however, the flow becomes compressible as indicated by an increase in the phase angle $\phi_{Vw\text{-}U}$ from zero, at around 750Hz, to nearly 90°. This relates to the relative magnitudes of the inertia and damping forces. In contrast, the phase angle between the internal pressure and the orifice velocity, $\phi_{Pi\text{-}U}$ is nearly constant around 90° over the entire frequency range. These findings are qualitatively and quantitatively in agreement with earlier measurements [18].

A further observation in Figures 6 and 7 is that while the phase angle $\phi_{Vw\text{-}U}$ is approximately zero at low frequencies, it is however around 180° at the higher frequencies, and in particular around the second resonant peak. This clearly implies that the diaphragm and orifice flow movements are in phase or in harmony with each other at the low frequencies. At the second resonance mode however, $\phi_{Vw\text{-}U} \approx 180°$ clearly implies that the diaphragm and orifice flow movements are out of phase. This behaviour is very similar to that of a two-degree of freedom mechanical system, consisting of two masses, two springs, and two dash-pots, connected in series.

The implication of these results is that the behaviour of the air in the actuator cavity is compressible not only around the Helmholtz frequency, but more so at all frequencies beyond the Helmholtz frequency. This is contrary to the general belief that compressibility may be important only when the actuator is driven around the Helmholtz resonance frequency of the cavity. This important result has significant implications for CFD modelling of synthetic jet actuators, especially when actuators are most efficiently driven at either resonance frequency.

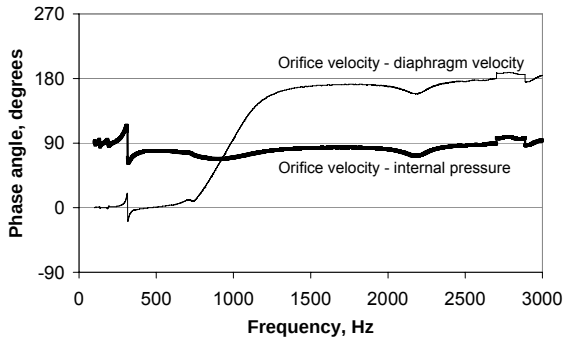

Figure 7. Calculated phase angles for Case I.

Influence of Cavity Volume

The influence of actuator cavity volume on the maximum orifice flow velocity for Case I is shown in Figure 8. The trends are similar to the LEM results of Gallas et al. [18], showing decrease in Helmholtz resonance and thus the first resonance frequency with increasing volume. This is accompanied by decreased response as the first and second resonance peaks become smaller with larger volume. A solution was also obtained for 21% of the nominal volume for case I, at which the Helmholtz resonance frequency is exactly equal to the diaphragm resonance frequency of 2114 Hz. While the maximum output velocity in this situation is slightly lower than that obtained for a 50% volume, a broad band response is nevertheless evident. The actuator output is relatively large over a wide frequency range, and such a condition may be desirable where the operating conditions might drift, or are not exactly determinable during design.

Influence of Diaphragm Natural Frequency

The influence of the diaphragm resonance frequency, physically achieved by adding 'mass' to the diaphragm, on the actuator output is shown in Figure 9. Two solutions were obtained, corresponding to increased diaphragm mass relative to Case I (see Table 1), one of which was 'tuned' so that the diaphragm natural frequency exactly equalled the Helmholtz resonance frequency of 977 Hz. Again, the actuator output is seen to be maximized when the two resonance frequencies are brought close to each other.

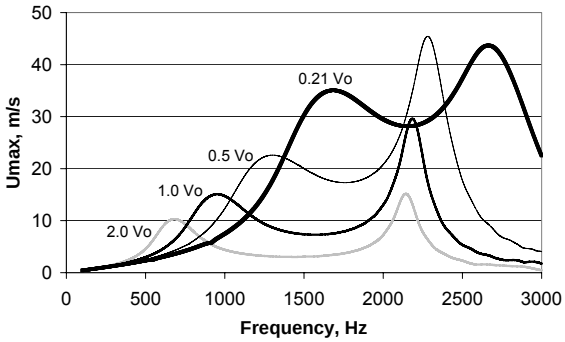

Figure 8. Predictions for varying cavity volume (Case I).

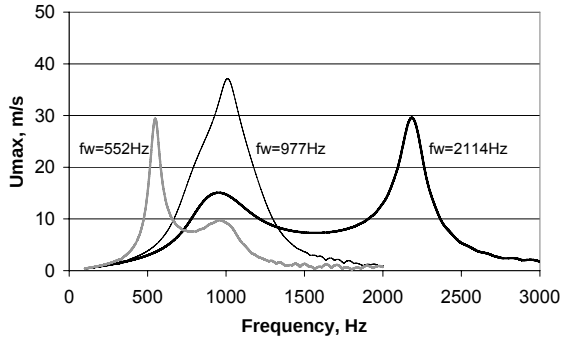

Figure 9. Predictions for varying diaphragm natural frequency (Case I).

Influence of Varying Steady External Pressure

Figure 10 compares the orifice velocities obtained for a number of different steady levels of external pressure p_e for an actuation frequency of 977Hz, which is the Helmholtz resonance frequency of the actuator cavity. The actuator output is known to be maximised at either the Helmholtz resonance frequency of the actuator, or at the oscillating wall natural frequency [15-18]. The diaphragm forcing amplitude was fixed at 0.5N. Except for the initial transient phase, the time histories are very much identical under continuous actuation. As expected [24-26], overshooting of the orifice velocity is seen to occur in the initial transient response, which becomes pronounced as the magnitude of p_e increases. As the initial cavity pressure has been set to zero gauge, the initial overshoot is represented by a negative orifice velocity, indicating an in-rush of air, which is obvious since the external pressure is above that of the cavity interior. Beyond the initial transients, the cavity internal mean pressure level attains the mean external pressure level, and actuation then produces cavity pressure fluctuations about these mean levels, with orifice velocity oscillations between +15m/s to -15m/s.

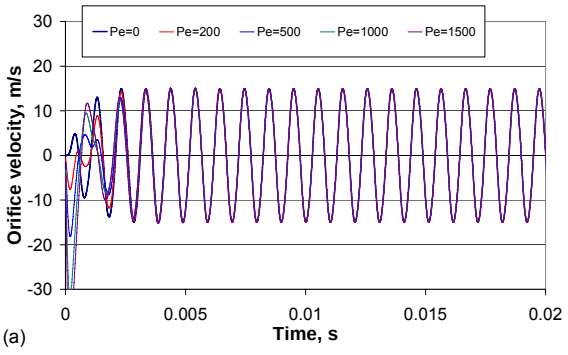

Figure 10. Orifice velocities with steady external pressure

Influence of External Pressure Fluctuations

The nature of the real fluctuations in pressure in the flow-field around a body can be complicated and dependent upon the location of the synthetic jet actuator for a particular application. Even then, it could be represented through a series sum of sinusoidal waveforms. In the present study, a sinusoidal form for $p_e(t)$ is used to provide insight into the behaviour of the actuator,

$$p_e = \overline{p}_e + A_{pe} \sin\left(2\pi f_{pe}\, t + \phi\right) \qquad (15)$$

in which $\overline{p}_e$, A_{pe} and f_{pe} are the mean level, amplitude and the fluctuation frequency of the external pressure signal respectively; while ϕ is the phase angle between the external pressure and the actuator forcing function.

Figures 11 compares orifice velocities when the external pressure p_e fluctuates with an amplitude of 100Pa about a mean level of 200Pa. The forcing and external pressure fluctuation frequencies (f and f_{pe}) were both set at 977Hz. The plot reveals that the orifice flow velocities are strongly sensitive to the phase relationship between p_e and the forcing function F. When p_e and the forcing function F are in phase (phase angle ϕ = 0), the maximum velocities obtained are much reduced relative to the steady external pressure situation. This is due to the fact with ϕ = 0°, when external pressure is increasing, the oscillating wall is being forced inwards, hence each effect tends to counter-act the other leading to a much reduced response. On the other hand, when ϕ = 180°, the largest fluctuations in orifice velocities are obtained. This makes sense since increases in p_e are accompanied by decreases in F and vice-versa, and the two effects tend to complement each other, resulting in a much enhanced response. A phase difference of ϕ = 90° results in maximum velocities between the latter and those from steady p_e.

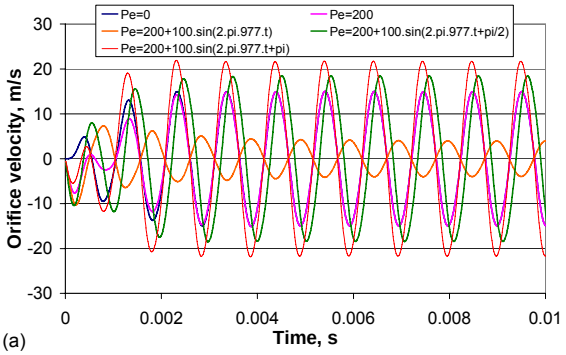

Figure 11. Orifice velocities with fluctuating external pressure

External Pressure Fluctuation Frequency Close to Helmholtz Frequency

Solutions were also obtained with actuator and external pressure oscillation frequencies being unequal. Figure 12 presents orifice velocities obtained with f = 977Hz and a number of different values for f_{pe}. Interestingly, this shows that relatively large orifice velocities can also be obtained with external pressure fluctuation frequencies much different to the actuation frequency. Figure 13 presents data for two cases where f is close to f_{pe}, namely (a) f = 977Hz, f_{pe}.= 970Hz; and (b) f = 970Hz, f_{pe}.= 977Hz. It shows an interesting actuator response, in which a high frequency fluctuation is superimposed upon a slowly varying component i.e. a modulating waveform. When this occurs, the actuator orifice velocity is maximised at only regular intervals, whilst at other times it may reach very small levels. From the synthetic jet actuation viewpoint, this might not be desirable, as the low velocities would not be sufficient to form a synthetic jet [28].

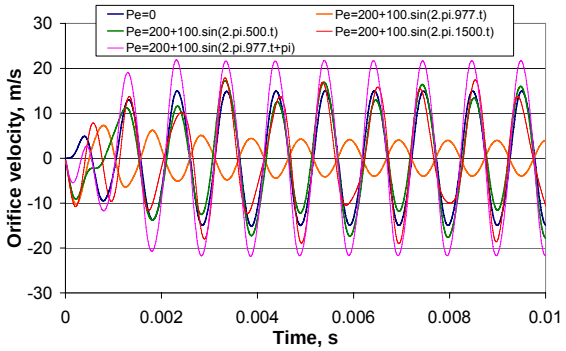

Figure 12. Orifice velocities with varying f_{pe}

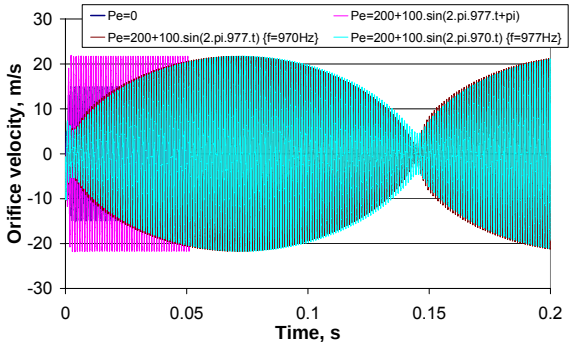

Figure 13. Orifice velocities for f_{pe} close to actuation frequency f

Frequency Response Characteristics with Fluctuating External Pressure

Some idea of the frequency response characteristics of the actuator is gained from the plot of maximum orifice velocities against frequency of actuation in Figure 14. These have been obtained by solving the model equations at each actuation frequency, and then extracting the maximum velocity from the time histories thus generated. Several forms for the external pressure were considered. It should be noted that in all these computations, the actuation force amplitude used was a consistent 0.5N (which is different from the 0.574N that used earlier). As noted earlier, Figure 14 shows that external pressure can have a profound effect on the response of the actuator, and in particular, the actuator output may in fact be enhanced over a wide frequency range. This plot must however be used with caution, as we have noted already the modulating orifice velocity form that may be obtained, and that over a certain frequency range about the external pressure fluctuation frequency, the actuator might be rendered ineffective in producing a continuous synthetic jet.

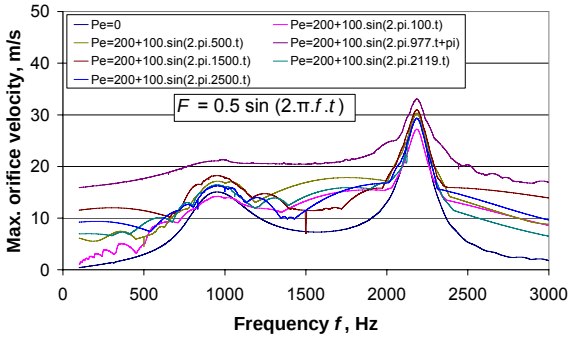

Figure 14. Frequency response of the actuator to varying external pressure signals

Conclusions

An analytical model for a synthetic jet actuator based on the laws of fluid dynamics has been developed and validated against experimental data in the published literature. The model is able to predict the performance and sensitivity of the actuator, defined by the orifice flow velocity, to changes of important design parameters, to diaphragm forcing input as well as to fluctuating external pressure stimulus at actuator orifice. It is also able to predict actuator cavity pressure variations and the phase relationships between the actuator wall movements and the orifice velocity.

The model and analysis based on it provide valuable insights into the behaviour of synthetic jet actuators, and reveals that the behaviour of the air in the actuator cavity is compressible at all frequencies from around the Helmholtz frequency and beyond. Furthermore, the model shows that actuator output velocity is maximised when the cavity Helmholtz and wall natural frequencies are brought together.

Analysis using the model also reveals that the performance of the synthetic jet actuator represented by the orifice velocity, is strongly dependent on fluctuations in the external flow. The magnitude and phase relationships between the external flow fluctuations and wall forcing function also play a key role in the actuator performance. With a phase difference of 180º between the actuator forcing and external pressure signals both oscillating at the same frequency, the actuator response is maximized. A modulating actuator output results when the forcing and external pressure frequencies are in the vicinity of each other, resulting in very low orifice velocities at repeating intervals. This would perhaps render the actuator ineffective in generating a synthetic jet. Limited frequency response computations also reveal some interesting differences in the performance of synthetic jet actuators operating into a fluctuating flow-field relative to that into quiescent air.

Acknowledgments

The grant support from the Research Committee as well as the Vice Chancellors University Development Funds of the University of Auckland is gratefully acknowledged.

References

[1] James, R. D., Jacobs, J. W., and Glezer, A., "A round turbulent jet produced by an oscillating diaphragm," *Physics of Fluids*, **8 (9)**, 1996, pp. 2484-2495.

[2] Smith, B. L., and Glezer, A., "The formation and evolution of synthetic jets", *Physics of Fluids*, **10 (9)**, 1998, pp. 2281-2297.

[3] Glezer, A., and Amitay, M., "Synthetic jets," *Annual Review of Fluid Mechanics*, **34**, 2002, pp. 503-529.

[4] Smith, D., and Glezer, A., "Vectoring and small-scale motions effected in free shear flows using synthetic jet actuators," AIAA paper 98-0209, 1998.

[5] Davis, S. A., and Glezer, A., "Mixing control of fuel jets using synthetic jet technology," AIAA paper 99-0447, 1999.

[6] Crook, A., Sadri, A. M., and Wood, N. J., "The development and implementation of synthetic jets for the control of separated flow," AIAA paper 99-3176, 1999.

[7] Smith, D. R., "Interaction of a synthetic jet with a crossflow boundary layer," *AIAA Journal*, **40**, 2002, pp. 2277-2288.

[8] Benchiekh, M., Bera, J-C., Michard, M., and Sunyach, M., "Contróle par jet pulse de l'écoulement dans un divergent court à grand angle,". *Mécanique des fluids/Fluid mechanics:C. R. Acad. Sci. Paris*, t.328, 2000, Série II b, pp. 749-756.

[9] Amitay, M., Pitt, D., Kibens, V., Parekh, D., and Glezer, A., "Control of internal flow separation using synthetic jet actuators," AIAA paper 2000-0903, 2000.

[10] Amon, C. H., Murthy, J., Yao, S. C., Narumanchi, S., Wu, C., and Hsieh, C., "MEMS enabled thermal management of high heat flux devices (EDIFICE)," *Experimental Thermal and Fluid Science*, **25**, 2001, pp. 231-242.

[11] Traniček, Z., and Tesař, V., "Annular synthetic jet used for impinging flow mass transfer," *International Journal of Heat and Mass Transfer*, **46**, 2003, pp. 3291-3297.

[12] Mallinson, S.G., Hong, G., and Reizes, J. A., "Some characteristics of synthetic jets," AIAA paper 99-3651, June 1999.

[13] Guy, Y., T. McLaughlin, E., and Albertson, J. A., "Velocity measurements in a synthetic jet," AIAA paper 2000-0118, 2000.

[14] Guy, Y., McLaughlin, T. E., and Albertson, J. A., "Effect of geometric parameters on the velocity output of a synthetic jet actuator," AIAA paper 2002-0126, 2002.

[15] Gallas, Q., Mathew, J., Kaysap, A., Holman, R., Nishida, T., Carroll, B., Sheplak, M., and Cattafesta, L., "Lumped element modeling of piezoelectric- driven synthetic jet actuators," AIAA paper 2002-0125, Jan 2002.

[16] Gallas, Q., Holman, R., Nishida, T., Carrol, B., Sheplak, M., and Cattafesta, L., "Lumped element modeling of piezoelectric- driven synthetic jet actuators," *AIAA Journal*, **41(2)**, 2003, pp. 240-247.

[17] Gallas, Q., Wang, G., Papila, M., Sheplak, M., and Cattafesta, L., "Optimisation of Synthetic jet actuators," AIAA paper 2003-0635, Jan 2003.

[18] Gallas, Q., Holman, R., Raju, R., Mittal, R., Sheplak, M., and Cattafesta, L., "Low dimensional modeling of zero-net mass-flux actuators," AIAA paper 2004-2413, July 2004.

[19] Sharma, R.N., Fluid-Dynamics-Based Analytical Model for Synthetic Jet Actuation, *AIAA Journal*, **45(8)**, 2007, 1841-1847.

[20] Sharma, R.N., An Analytical Model For Synthetic Jet Actuation Into An External Flow Field', Paper Number AIAA-2007-3850, Proc of the 37th AIAA Fluid Dynamics Conference, 25-28 June 2007, Miami, USA

[21] Kinsler, L. E., Frey, A. R., Coppens, A. B., and Sanders, J. V., *Fundamentals Of Acoustics*, 4th Ed., John Wiley & Sons Publishers USA, 2000, pp. 184-187.

[22] Hall, D. E., *Basic Acoustics*, Harper & Row Publishers NY USA, 1987, pp. 107-109; pp. 235-243.

[23] Etheridge, D. W., "Nondimensional methods for natural ventilation," *Building and Environment*, **37**, 2002, pp. 1057-1072.

[24] Sharma, R. N., and Richards, P. J., "Computational modelling of the transient response of internal pressure to a sudden opening," *Journal of Wind Engineering and Industrial Aerodynamics*, **72**, 1997, pp.149-161.

[25] Vickery, B. J., "Internal pressures and interactions with the building envelope," *Journal of Wind Engineering and Industrial Aerodynamics*, **53**, 1994, pp. 125-144.

[26] Sharma, R. N., and Richards, P. J., "Computational Modelling in the Prediction of Building Internal Pressure Gain Functions," *Journal of Wind Engineering and Industrial Aerodynamics*, **67-68**, 1997, pp. 815-825.

[27] Press, W. H., Flannery, B. P., Teukolsky, S. A., and Vetterling, W. T., *Numerical Recipes in C: The Art of Scientific Computing* (*2nd Edition*), Cambridge University Press, 1992, pp. 710-714.

[28] Utturkar, Y., Holma, R., Mittal, R., Carrol, B., Sheplak, M, Cattafesta, L., "A jet forma-tion criterion for synthetic jet actuators," AIAA paper 2003-0636, 2003.